Geotechnical Engineering Journal of the SEAGS & AGSSEA Vol. 48 No. 4 December 2017 ISSN 0046-5828

Soil-Water Coupled Analysis of Pore Water Pressure Dissipation in Performance Design—Examinations of Effectiveness in Reclaimed Ground

Toshihiro Nonaka[1], Shotaro Yamada[2] and Toshihiro Noda[2]
[1]*Disaster Mitigation Research Center, Nagoya University, Nagoya, Japan*
[2]*Department of Civil Engineering, Nagoya University, Nagoya, Japan*
E-mail: nonaka@nagoya-u.jp

ABSTRACT: Japan has a large number of reclaimed regions unimproved against liquefaction and countermeasures in such regions are necessary to prepare for a great earthquake. A new macro-element method has been proposed that involves applying the soil-water-coupled finite deformation analysis code ***GEOASIA*** with an inertial term, and a numerical-analysis technique has been designed that quantitatively evaluates the improvement effect of the pore water pressure dissipation method (PWPDM). In this study, PWPDM effectiveness was examined for a reclaimed ground using the proposed method. Detailed examinations were conducted with the intention of developing a more advanced performance design, without being limited to the concept of the current design code. The main findings are as follows: 1) the proposed analysis code enables quantitative evaluation of the improved effectiveness of PWPDM in a reclaimed ground; 2) more advanced PWPDM designs are possible by not only suppressing the maximum excess pore water pressure to the permissible range of the current design code, but also evaluating the ground deformation adequately; and 3) the new macro-element method, capable of reproducing the phenomenon of well resistance, can evaluate the reduction in the improvement effect because of the degradation of drainage capability, thus making it useful for maintenance purposes such as drain clogging.

Keywords: Pore water pressure dissipation, Soil-water coupled analysis, Macro-element method, Reclaimed ground, Performance design

1. INTRODUCTION

Japan is a country with limited area and a long history of reclaiming land from ocean areas. Reclamation projects have accelerated since the beginning of Japan's high economic growth period and important social capital has been constructed on these reclaimed grounds (Yasui et al. 2002); however, there are significant concerns regarding the liquefaction damage caused by great earthquakes on such grounds, which are generally softer than natural ground. Therefore, countermeasures are required to be taken as soon as possible in these regions. The vicinities of many important structures have been improved using highly reliable liquefaction countermeasures, such as sand compaction pile method. However, relatively low-priority areas, such as reclaimed piers, have remained unimproved. It is desirable to choose a method that is relatively inexpensive and superior in feasibility because the reclaimed ground to be improved is so extensive. One such method that satisfies these requirements is the pore water pressure dissipation method (PWPDM). A liquefaction countermeasure using artificial drains was applied in a section of Tokyo Lumber Terminal 15 during the period from 2001 to 2005, and reports indicated that this section escaped the liquefaction damage caused during the 2011 Great East Japan Earthquake, as shown in Figure 1 (Research Association for DEPP Method 2011).

Unimproved region Improved region

Figure 1 Liquefaction countermeasure effect of PWPDM (Research association for DEPP Method 2011)

Research on the PWPDM was spurred by Seed and Booker's proposal (1977) for a design method for gravel piles, and numerous efforts have been made and model experiments have been conducted to explain the mechanisms. On the basis of the results of one-gravity (1G) shaking-table tests, Tanaka et al. (1987) proposed an equation to estimate the excess pore water pressure (EPWP) occurring in improved ground with gravel piles during an earthquake along with a method for estimating settlement of ground surface. Adalier et al. (2003) conducted a centrifugal-model test simulating a ground with concentrated load and showed that suppressing the increase in EPWP maintained the stiffness of the overall ground, thus reducing the settlement caused by the concentrated load.

Some numerical approaches to PWPDM has been developed using the effective stress analysis code FLIP by Tashiro et al. (2015) and the two-dimensional finite difference code FLAC by Papadimitriou et al. (2007). However, there have been few attempts to measure PWPDM effectiveness based on numerical analysis at the research level, let alone at the working level. Numerical modeling of this method has made little progress compared with the experimental approach, primarily because of the following two challenges. The first one is predicting the degree of deformation that can occur as a result of the suppression of increasing EPWP during an earthquake. Moreover, handling consolidation after an earthquake in a consistent manner is necessary; however, few analysis codes can satisfy these requirements. The second challenge is finding methods to improve the calculation efficiency. Most conventional numerical analyses require three-dimensional (3D) fine meshes to represent a large number of drains installed in the ground, resulting in an enormous calculation cost. Therefore, finding a way to avoid this cost has become a key issue. For example, Tashiro et al. (2015) conducted plane-strain analysis by expressing drains as permeable boundaries and converting the horizontal permeability coefficient from an axi-symmetric condition. However, this method requires a fine mesh and is laborious to a certain extent as the improved area must be re-meshed and the permeability coefficients must be re-calculated whenever the drain spacing is changed. Moreover, the well resistance effect is not considered by this method. Papadimitriou et al. (2007) represented the drains by increasing the permeability coefficient of the finite elements; however, even this method requires a 3D fine mesh. The challenges described above are considered as the main reasons for a wide-scale numerical analysis of actual reclaimed ground not having been conducted till date. More specifically, improvement of the reliability of PWPDM has been hobbled by the lack of an effective analytical method capable of resolving these two problems.

To resolve these problems, Yamada et al. (2015) extended the function of the macro-element method (Sekiguchi et al. 1986), which is a type of homogenization method, and Noda et al. (2015)

applied it to the soil-water coupled finite deformation analysis code ***GEOASIA*** (Noda et al. 2008) with an inertial term. ***GEOASIA*** is capable of uniformly handling the following phenomena: 1) both compaction and liquefaction and 2) both compaction settlement during an earthquake and consolidation settlement after liquefaction. Therefore, it can predict the degree of deformation during and after an earthquake through PWPDM simulation. As this code is based on the finite deformation theory, it is able to accurately simulate the case with large deformation. Furthermore, since the macro-element method introduces the water absorption functions of a drain into individual elements, it can simulate the PWPDM without fine meshing.

Oka et al. (1992) and Kato et al. (1994) carried out a pioneering numerical analysis of the PWPDM using a macro-element method. They introduced the original macro-element method proposed by Sekiguchi et al. (1986) into LIQCA (Development group of liquefaction analysis code LIQCA 2004), a computer program for liquefaction analysis, to examine the effects of suppression and dissipation by gravel drains upon EPWP. To approximately account for well resistance, which indicates the drainage resistance of drains, they also multiplied the discharge index from soil to drains by a correction coefficient based on the findings of Tanaka et al. (1983). In contrast, the new macro-element method (Yamada et al. 2015; Noda et al. 2015) employed in this study considers the water pressure inside the drain as unknown and provides simultaneous solutions for ground motion and pore water pressure. As a result, well resistance is automatically generated by a series of calculations depending on the given conditions. In this method, the drain spacing can be set to any value not by using a different mesh but by varying the material constants of the macro-element method. For an explanation of the new macro-element method, see Appendix A. Furthermore, comparing the results of a 3D mesh-based analysis in which drains were expressed exactly by finely dividing a finite-element mesh with those of a two-dimensional (2D) mesh-based analysis using the new macro-element method indicated that the 2D model with the new macro-element method approximated the 3D model accurately in terms of EPWP change and settlement of ground surface (Noda et al. 2015).

The PWPDM design is as discussed below. PWPDM is a method aimed at suppressing the increase in EPWP; however, the improving effect considerably decreases once EPWP increases to a high level. Therefore, geotechnical engineers have been focusing on suppressing the water pressure within the permissible range specified in the current design code. In contrast, Howell et al. (2012) demonstrated, through shaking-table tests of drains installed on gentle slopes, that the installation of a drain provided a certain suppressive effect on liquefaction and residual deformation, even if the EPWP ratio exceeded the permissible value during an earthquake. Unno et al. (2012) made a similar suggestion. These studies were limited to a simple evaluation using a model test; however, a more advanced performance design of PWPDM must be developed to quantitatively evaluate the suppressive effect of liquefaction through numerical analysis in cases where the EPWP ratio exceeds the permissible value specified in the current design code.

In this study, the authors attempted to quantitatively evaluate the suppressive effect of liquefaction in the case where the maximum EPWP ratio exceeds the permissible value specified in the current design code by estimating the improved effect of PWPDM in an actual reclaimed ground using ***GEOASIA*** with the new macro-element method. No previous studies have been conducted a wide-scale numerical analysis of an actual ground while making use of a macro-element method. Certain amount of suppressive effect of liquefaction can be expected to occur even if the EPWP ratio exceeds the permissible value; for instance, ground deformation and localized settlement by a superstructure are suppressed as a result of the suppression of increase in EPWP and promotion of dissipation in EPWP during an earthquake by the discharge function of the drain. The new macro-element method, which treats the water pressure inside the drain as an unknown, can evaluate the deterioration in the permeability of a drain through processes such as drain clogging.

2. ANALYTICAL EXAMINATION USING 1D MESH

Noda et al. (2015) showed that the design procedure for PWPDM could be streamlined by first determining the range of effective drain spacing using a one-dimensional (1D) mesh-based analysis, prior to performing 2D and 3D mesh-based soil-water coupled analyses with the macro-element method. In this section, according to this procedure, some specific values of the drain spacing will be selected by 1D mesh-based analysis. The case where the EPWP ratio exceeds the permissible value specified in the current design code will be also examined. Furthermore, the ***GEOASIA*** with the new macro-element method will be validated by comparing with the empirical formula of settlement based on shaking-table tests.

2.1 Analytical conditions

The target of this analysis was an actual reclaimed ground in Nagoya harbor that was addressed by Noda et al. (2010). This reclamation was completed in the 1960s, so it was not affected by any great earthquakes such as the 1944 Tonankai Earthquake or the 1946 Nankai Earthquake. Since the ground was reclaimed without any particular seismic countermeasures, it is quite vulnerable to a great earthquake. Figure 2 shows the 1D finite-element mesh. The figure also provides the boundary conditions used for the analysis.

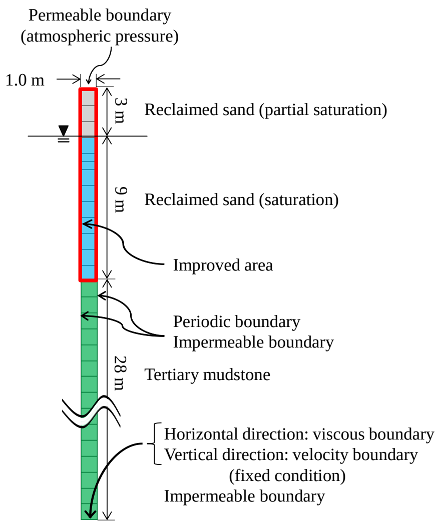

Figure 2 Finite element mesh and boundary condition (1D mesh)

First, a 28-m-thick layer of tertiary-period mudstone was laid on the bedrock. Next, the sand was reclaimed. The groundwater level was at a depth of 3 m below the ground surface. The hydraulic condition for the upper surface was a permeable boundary, and the sides and bottom of the ground were assumed to be impermeable. Viscous boundaries (Lysmer and Kuhleemeyer 1969; Noda et al. 2009) were applied in the horizontal direction at all the nodes along the bottom boundaries, and their material constants were set based on a PS logging result. A periodic boundary condition was applied to the side boundaries. SYS Cam-clay model (Asaoka et al. 2002), an elasto-plastic constitutive model, was used in the analysis. This model is capable of describing, within a single theoretical framework, the behaviors of sands, clays, and intermediate soils by introducing the works of soil skeleton structures (structure, overconsolidation, and anisotropy). This model is equally capable of handling liquefaction and compaction as the phenomena resulting from the degradation of the structure and the accumulation of overconsolidation. Therefore, this model makes it possible to predict the degree of deformation during an earthquake using PWPDM. The macro-element method was applied to the elements in the region enclosed by the bold red line frame in the Figure 2 to represent the ground improved by PWPDM. A spiral drain (Research Association for DEPP Method 2011), was assumed to be used in the PWPDM.

Table 1 shows the material constants and initial values for the ground used in this analysis (including values for the ripraps used in the next section). These values were determined from the specimens sampled from this site by Noda et al. (2010). The elasto-plastic parameters shown in Table 1 were determined from triaxial compression and consolidation tests using disturbed specimens. Moreover, the evolution parameters were determined by simulating the mechanical behavior of undisturbed specimens through the SYS Cam-clay model. Figure 3 and 4 present examples of the behaviors of the sand sampled from the reclaimed ground in undrained compression tests and dynamic deformation characteristics, as well as the reproductions of these tests by the SYS Cam-clay model. The results of the undrained compression tests under different confining pressures are well reproduced using the set of material constants given in Table 1. Turning to the initial conditions, the specific volume and degree of structure within each layer of ground were assumed to be uniform. The overconsolidation ratio was distributed according to the overburden pressure (Noda et al. 2005). The soil-particle density of the unsaturated part of the reclaimed ground was decided such that the saturated unit weight of this part was equal to the wet unit weight under 30% saturation. All calculations used the mesh as shown in Figure 2. A useful feature of the macro-element method proposed by the authors is that the drain spacing can be changed without using different meshes and by simply varying the equivalent diameter d_e, which is a material constant in the macro-element method, without degrading the approximate accuracy (Noda et al. 2015).

The viscous boundary condition was applied in the horizontal direction to all nodes at the bottom boundary. Table 2 provides the material constants for the viscous boundary condition. Tokai, Tonankai, and Nankai-linked-type earthquakes (Cabinet Office 2004) were reported to occur offshore of this region. Figure 5 shows the seismic motion assumed by this type of a subduction-zone earthquake. In this scenario, the motion contains many long-period components. The maximum acceleration of this motion was approximately 250 gal, and the duration of the principal motions was quite long at approximately 100 s. This wave was input on the viscous boundary.

Note here that, although the initial stress ratios in the reclaimed sand were simply set to zero, the deformation analysis results were hardly affected by the initial stress ratio within 0 to 0.545.

Table 1 Material constants and initial values (Noda et al. 2010)

	Tertiary mudstone	Riprap	Coating riprap	Reclaimed sand (saturation)	Reclaimed sand (partial saturation)
Elasto-plastic parameters					
Critical state index M	0.60	1.70	1.70	1.10	1.10
NCL intercept N	2.10	1.895	1.895	1.989	1.989
Compression index $\tilde{\lambda}$	0.17	0.105	0.105	0.05	0.05
Swelling index $\tilde{\kappa}$	0.003	0.0005	0.0005	0.0002	0.0002
Poisson's ratio v	0.3	0.3	0.3	0.3	0.3
Evolution parameters					
Ratio of $-D_v^p$ to $\|\boldsymbol{D}_s^p\|$ c_s	1.0	1.0	1.0	1.0	1.0
Degradation index of structure a	0.01	2.0	2.0	5.0	5.0
Degradation index of OC m	10.0	1.20	1.20	0.12	0.12
Rotational hardening index b_r	0.001	1.0	1.0	3.0	3.0
Limitation of rotational hardening m_b	1.0	0.001	0.001	0.9	0.9
Fundamental parameters					
Soil particle density ρ_s (g/cm^3)	2.707	2.593	2.593	2.675	2.035
Permeability index k (cm/s)	1.0×10^{-7}	1.0×10^{-3}	1.0×10^{-3}	4.0×10^{-3}	4.0×10^{-3}
Initial conditions					
Specific volume v_0	1.70	1.593	1.062	1.914	1.914
Stress ratio η_0	0.545	0.0	0.0	0.0	0.0
Degree of structure $1/R^*_0$	50.0	1.0	1.0	1.4	1.4
Degree of anisotropy ζ_0	0.0	0.0	0.0	0.7	0.7

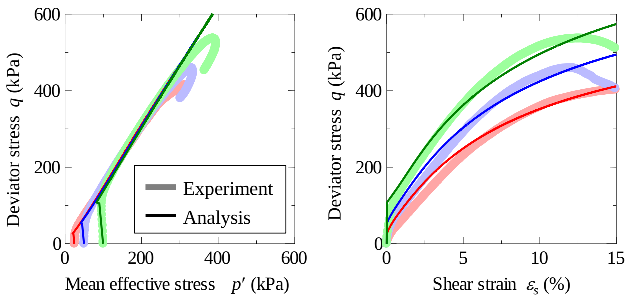

Figure 3 Behavior of undrained compression test of reclaimed sand and reproduction analysis by SYS Cam-clay model

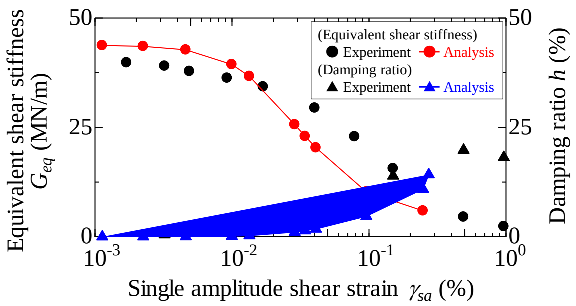

Figure 4 Behavior of dynamic deformation characteristics of reclaimed sand and reproduction analysis by SYS Cam-clay model

Table 2 Material constants of viscous boundary

Bedrock density ρ (g/cm^3)	2.0
S-wave velocity in bedrock Vs (m/s)	570.0

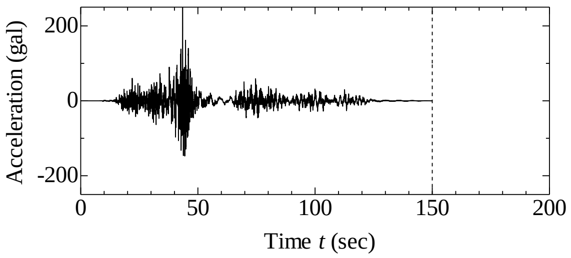

Figure 5 Input seismic motion

2.2 Influence of drain spacing upon the improvement effect

Figure 6 shows the relation between the drain spacing and maximum EPWP ratio. This ratio was found at a depth of 6.5 m below the groundwater level. The diameter of the circular drain, d_w, was 0.1 m and its permeability coefficient, k_w, was 7.0×10^2 cm/s. k_w is a new parameter that has been added owing to the incorporation of the discharge function of the drains in the macro-element method, which was not in the original macro-element method. In the conventional analysis method where drains were represented by dividing element meshes, the permeability coefficient of element was difficult to be set to large values during the earthquake because of the restriction involved in ***u-p*** formulation. However, the permeability coefficient of drain in the new macro-element method, which is not restricted by ***u-p*** formulation, can be set to any value (for a detailed explanation, see Appendix A).

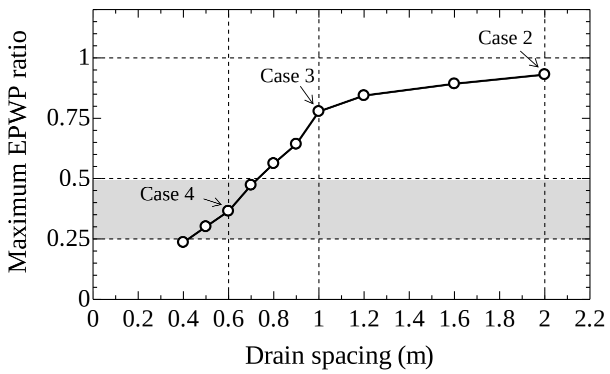

Figure 6 Relation between drain spacing and maximum EPWP ratio

As can be seen, closer the drain spacing, greater the suppression of increase in EPWP. In the current design code, the permissible maximum EPWP ratio during an earthquake is usually set in the range of 0.25–0.5 when assuming Level-1 seismic motions (Research Association for DEPP Method 2011). According to the design code, the effective drain spacing is within the range of 0.4–0.7 m. However, liquefaction countermeasures with this range of drain spacing may possibly be safer than necessary. As mentioned earlier, through the shaking-table tests, Howell et al. (2012) and Unno et al. (2012) proposed that the discharge function of the drain provided a certain suppressive effect on liquefaction, even if the maximum EPWP ratio exceeded the permissible value. Therefore, the effective drain spacing should be decided by considering not only the maximum EPWP ratio but also the ground deformation. Accordingly, for the cases where d = 0.6 m (which is within the permissible range) and d = 2.0 m and 1.0 m (which are outside of it) as targets, the change of EPWP and settlement of the ground surface were examined in detail through numerical analysis. No previous studies have quantitatively examined the improvement effect of PWPDM through numerical analysis in a case where the EPWP ratio exceeds the permissible value specified in the current design code.

2.3 Results of analysis

The suppression effects of liquefaction for d = 2.0 m, 1.0 m, and 0.6 m were examined in detail and compared with the effects observed for an unimproved region. Table 3 provides the list of analysis cases and material constants for the macro-element method (including Case 5 used in the Section 4).

Figure 7 shows the relation between time and EPWP ratios of the elements at a depth of 6.5 m below groundwater level. The ratio had increased to almost 1.0 approximately 20 s after the earthquake in Case 1, corresponding to liquefaction. In Case 4, however, the suppression of increase and the promotion of dissipation in EPWP occurred noticeably; that is, liquefaction was suppressed. In Cases 2 and 3, the EPWP ratio turned from increase to decrease at approximately 40 s, when the input acceleration reached a maximum. As shown in this figure, liquefaction was suppressed in Cases 2 and 3 compared with Case 1.

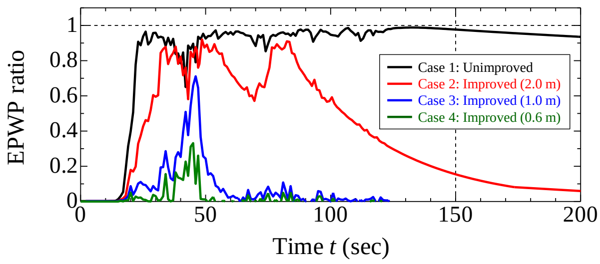

Figure 7 Relation between time and EPWP ratio

Figure 8 shows the variation in the excess water pressure of the ground and the drain in the depth direction. As can be seen, there is almost no increase in the drain water pressure in Cases 3 and 4, whereas the pressure is observed to increase in Case 2, although not significantly. This increase was attributed to the increase in the flow rate of water from the soil to a drain. However, the fact that the increase in water pressure was low even in Case 2 suggests that well resistance is unlikely to be a key issue when using drain materials with a high drainage capability, such as the spiral drain employed in this study.

To examine the behavior of the soil elements in the ground, the relations between the mean effective stress and specific volume in each case were compared. The soil elements examined here were at a depth of 6.5 m below groundwater level. Figure 9 shows the behavior of the elements.

Table 3 List of analysis cases and material constants of macro-element method

	Case 1	Case 2	Case 3	Case 4	Case 5
Drain spacing d (m)	— (Unimproved)	2.0 (Improved)	1.0 (Improved)	0.6 (Improved)	1.0 (Improved)
Equivalent diameter d_e (m)	—	2.26	1.13	0.68	1.13
Diameter of circular drain d_w (m)	—	0.10	0.10	0.10	0.10
Permeability coefficient of circular drain k_w (cm/s)	—	7.0×10^2	7.0×10^2	7.0×10^2	1.0×10^1

In Case 1, the mean effective stress was found to reduce to almost zero during an earthquake accompanied by an increase in EPWP, indicating a behavior leading to liquefaction. In contrast, the mean effective stress hardly decreased as a result of the drastic suppression of EPWP increase in Case 4.To compensate for the suppression of increase in EPWP, compression owing to compaction occurred during the earthquake. In Cases 2 and 3, the mean effective stress recovered with compression due to compaction during the earthquake, though it decreased to a certain degree. Therefore, ground-bearing capacity was also expected to be available in Cases 2 and 3. After the earthquake, remarkable compression occurred in Case 1 because of EPWP dissipation via consolidation. In Cases 3 and 4, however, there was almost no compression after the earthquake as dissipation of EPWP was almost complete by the end of the earthquake.

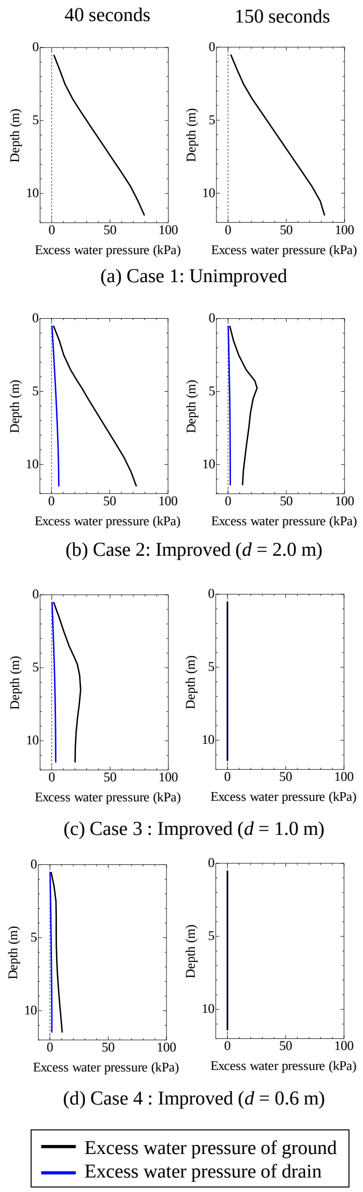

Figure 8 Excess water pressure in the depth direction

Figure 10 shows the relation between time and settlement of ground surface. In Case 1, there was little settlement during the earthquake but approximately 15 cm of settlement occurred owing to EPWP dissipation via consolidation. In contrast, EPWP was suppressed in Cases 2-4, resulting in the occurrence of settlement. However, little settlement via consolidation occurred in these cases because the dissipation of EPWP was almost complete by the end of the earthquake. Furthermore, the ultimate settlements were suppressed in the improved cases, and it was found that closer the drain spacing, greater the suppression of the settlement. In the drain-spacing case, where the maximum EPWP ratio exceeded the permissible value, the settlement of the ground surface was suppressed compared with that in the unimproved case. The settlement curves in Cases 3 and 4 were not smooth. This was because the function of drain was exerted instantly and settlement proceeded rapidly when the water pressure notably increased accompanied by major accelerations of input seismic motion.

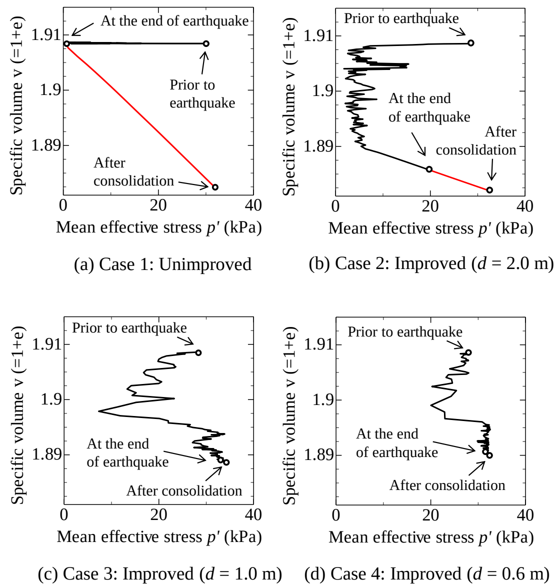

Figure 9 Relationships between the mean effective stress and the specific volume

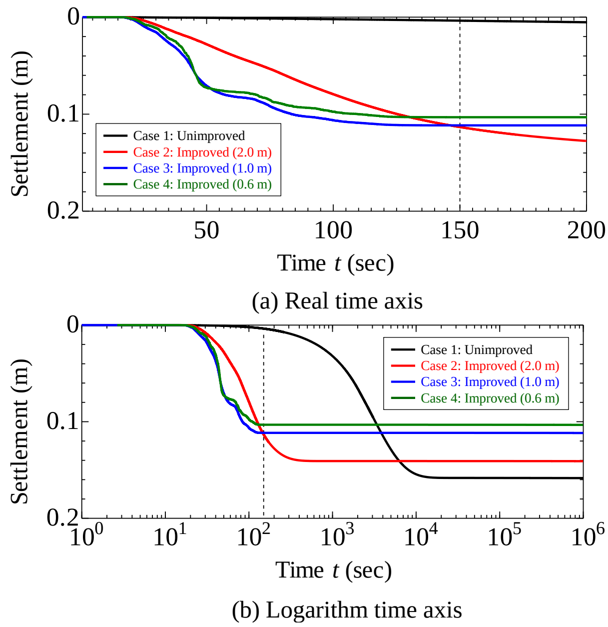

Figure 10 Time-settlement of ground surface

This indicates that an adequate liquefaction-suppressive effect is provided to the reclaimed ground using countermeasures with drain spacing ensuring that the maximum EPWP ratio falls within the permissible range specified in the current design. However, a certain degree of suppressive effect of liquefaction is provided, such as the increase in density and suppression of settlement occur as a result of the suppression of increase and the promotion of dissipation in EPWP during an earthquake by the discharge function of drain, even in the case of drain spacing where the maximum EPWP ratio exceeds the permissible value.

2.4 Validation of the new macro-element method

On the basis of the results of the 1G shaking-table tests applying PWPDM, Ono et al. (2009) and Unno et al. (2014) proposed an empirical formula for the settlement of the ground surface. For a detailed explanation of this formula, see Appendix B. The influence of well resistance is considered in this formula and used for designing PWPDM in Japan (Research Association for DEPP Method 2011). The analysis code ***GEOASIA*,** which employs the new macro-element method, was validated by comparing the settlements of several 1D mesh-based analyses shown in section 2.2 and analyses where the permeability coefficient of ground changed with those of the empirical formula.

Figure 11 shows the relation between the settlement calculated by the analysis code and that obtained by the empirical formula. The two values were observed to be generally same for several cases where drain spacing and permeability coefficient of ground were changed, although there was a tendency for the settlements obtained by the empirical formula to be larger than those calculated by the analysis code.

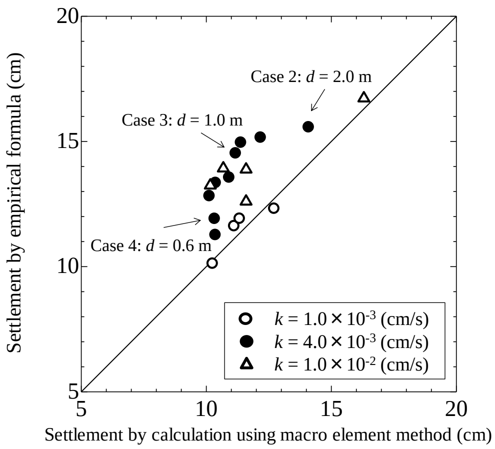

Figure 11 Relationship between calculation settlement and empirical formula settlement

3. EXAMINATION OF ANALYSIS USING 2D MESH

In an actual reclaimed ground, complicated ground deformation, i.e., localized settlement by superstructure, horizontal ground deformation including lateral flow caused by liquefaction. Hence, the suppressive effect of these deformations was investigated in detail using 2D mesh-based analysis, through which actual reclaimed ground, including revetment, was modeled. The limitations of evaluating the ground deformation using 1D mesh-based analysis were also examined by comparing settlements of ground surfaces in 1D and 2D mesh-based analyses.

3.1 Analysis conditions

Figure 12 shows the entire finite-element mesh, including the expanded mesh in the vicinity of the revetment. First, a 28 m-thick layer of tertiary-period mudstone was laid on the bedrock. Next, a rubble-mound revetment was constructed on top of this layer and the sand was reclaimed. The area considered for analysis was 2,040 m wide and 28 m high at the left end and 40 m high at the right end of the entire analysis region. Since this analysis was applied to a coastal structure, the hydraulic conditions for the upper surface of the ground were as follows: the region to the left of the revetment was assumed to be a permeable boundary determined by static water pressure and that to the right of the revetment was an atmospheric-pressure boundary. A simple shear boundary condition (Yoshimi et al. 2005) was applied to the side boundaries. Table 1 presents the material constants and initial values for the ground, Table 2 shows the material constants of the viscous boundary, and Figure 5 shows an input seismic motion. To simulate the effect of a structure built on the reclaimed ground, 18.5 kN/m concentrated loads were applied at the two locations shown in the figure. The revetment structure was modeled as a one-phase elastic body, the material constants for which are provided in Table 4. The new macro-element method was applied to the elements in the region enclosed by the bold red line frame in the figure. The width of the element in the improved region was 1.0 m, considerably rougher than that of the drain, and the drain spacing could be changed simply by varying the equivalent diameter d_e instead of using different meshes, similar to that done in 1D mesh-based analysis. Table 3 summarizes the analytical cases.

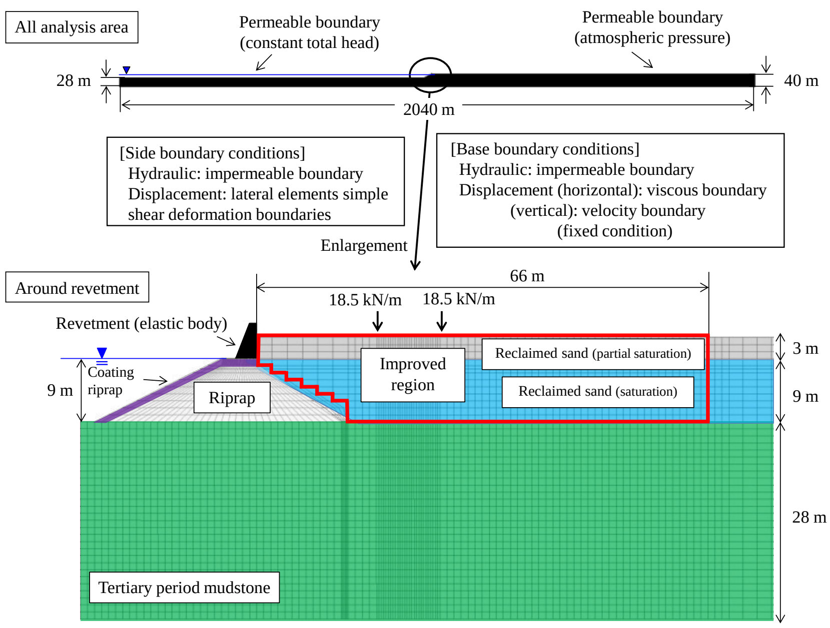

Figure 12 Finite element mesh and boundary condition (2D mesh)

Table 4 Material constants of revetment

Young's modulus E (kN/m^2)	2.35×10^7
Poisson's ratio v	0.20
Density γ (g/cm^3)	2.40

3.2 Results of analysis

Figures 13 and 14 show the distributions of EPWP and mean effective stress in Cases 1-4. The distribution of mean effective stress in Case 1 before earthquake is also showed (almost same distributions were confirmed in Case 2-4 before earthquake). In Case 1, the EPWP in the reclaimed sand monotonically increased from the beginning to the end of the earthquake, and the mean effective stress showed almost zero, i.e., liquefaction occurred. In contrast, the EPWP hardly increased and the mean effective stress was maintained at 40 s around the time of maximum seismic acceleration, and liquefaction was greatly suppressed over the entire improved region in Case 4. There was a lower suppressive effect on the increase of EPWP in Cases 2 and 3 compared with that in Case 4; however, the dissipation of EPWP, i.e., the recovery of mean effective stress progressed over the entire improved region until the end of the earthquake.

Figure 15 shows the shear strain distribution after consolidation. The large local shear strain that occurred in the vicinity of the concentrated load in Case 1 was suppressed in Cases 2-4. In addition, it was observed that closer the drain spacing, greater the suppression of the shear strain.

Next, Figure 16 shows the settlement of the ground surface at the end of earthquake and after consolidation. Broken lines in each figure show the settlements of the ground surface in the 1D mesh-based analysis. Comparing the 1D and 2D mesh-based analyses, settlements around the center of the improved region almost corresponded with one another, but settlements in the vicinity of the revetment and the border between the improved and unimproved regions were significantly different. At the end of the earthquake, there was approximately 30 cm of localized settlement in Case 1 for locations under concentrated loads. In Case 4, there was approximately 10–15 cm of settlement throughout the improved region; however, suppression of the increase in EPWP during the earthquake resulted in the suppression of the localized settlement. This was because the reclaimed sand never reached liquefaction and ground stiffness was maintained. In Cases 2 and 3, localized settlement was suppressed to a certain degree depending on drain spacing. In Case 1, after consolidation, approximately 20 cm of settlement occurred throughout the area owing to the EPWP process. However, this was almost non-existent in Cases 2-4, thereby indicating that the ultimate settlement throughout the improved region had been suppressed.

Figure 17 shows the horizontal displacement of the ground surface after consolidation (leftward displacement is positive). In the vicinity of the revetment, closer drain spacing corresponds to greater suppression of the horizontal displacement, that is, lateral flow was suppressed. However, the horizontal displacements in the improved cases were greater than unimproved case in the vicinity of the border between the improved and unimproved regions. Figure 18 shows the distributions of velocity vector in the reclaimed sand layer during earthquake in Cases 1 and 4. In Case 1, a whole reclaimed sand layer was moved to the left by lateral flow. On the contrary, in Case 4, the ground in the vicinity of the border was dragged to the left by the settlement in the improved region during the earthquake. Therefore, the horizontal displacements in the improved cases were greater in the vicinity of the border owing to the complexed effect caused by lateral flow and drawing.

These results indicate that certain suppressive effects of localized settlement and lateral flow were provided as a result of the promotion of dissipation of EPWP, even in the drain-spacing case where the maximum EPWP ratio exceeds the permissible value. In this study, the case of d = 1.0 m is sufficient as a countermeasure because there are few differences between the results at d = 1.0 m and 0.6 m in terms of suppression of ground deformation.

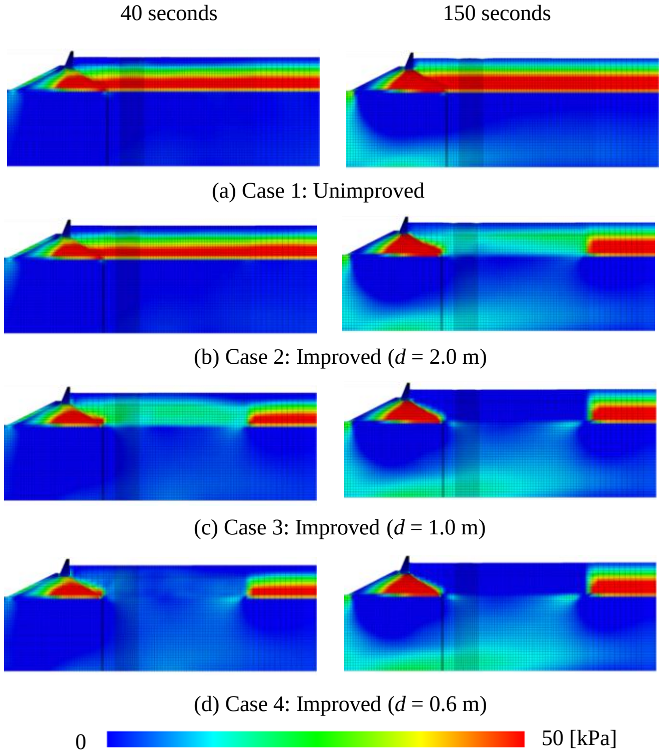

Figure 13 Distributions of EPWP

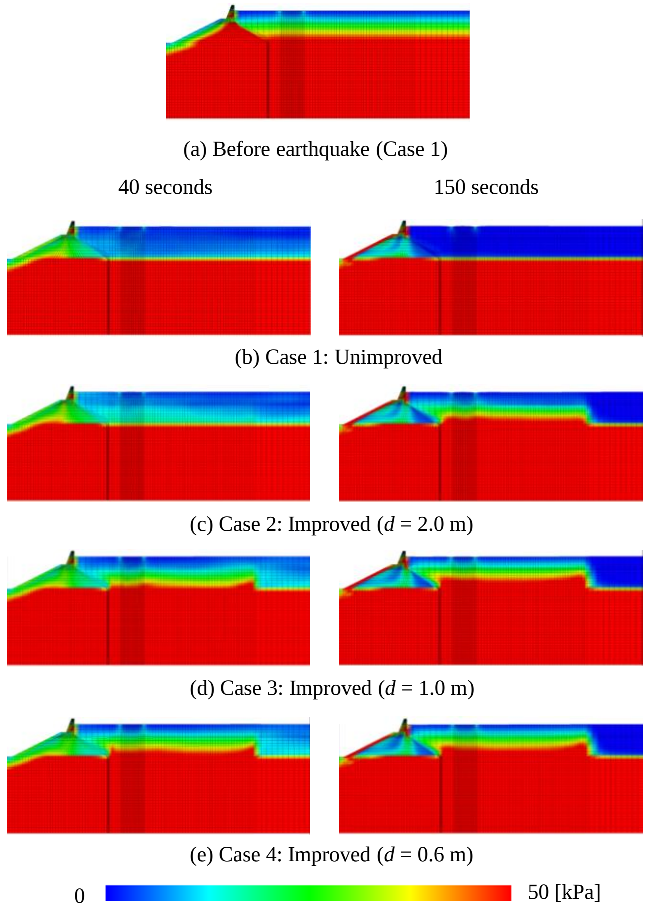

Figure 14 Distributions of mean effective stress

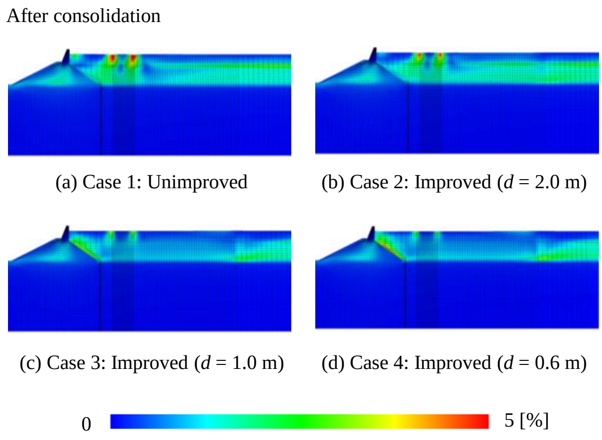

Figure 15 Distributions of shear strain

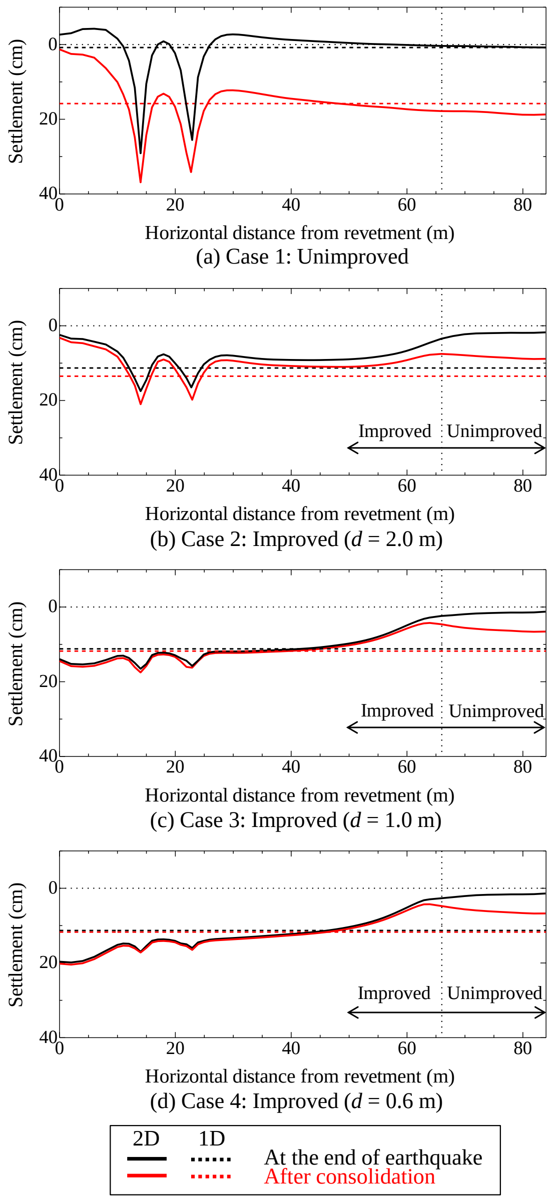

Figure 16 Settlement of ground surface

Developing a more advanced performance design is possible by not only suppressing the maximum EPWP within the permissible value in the current design code but also evaluating the ground deformation using a numerical analysis code, which enables quantitative evaluation of the improvement effect of PWPDM. For countermeasures in an extensive region such as a reclaimed ground, the effective drain spacing should be decided such that it does not exceed the necessary safety requirements in terms of the importance of the target point and the construction cost. The macro-element method applied to ***GEOASIA*** can effectively implement this more advanced performance design.

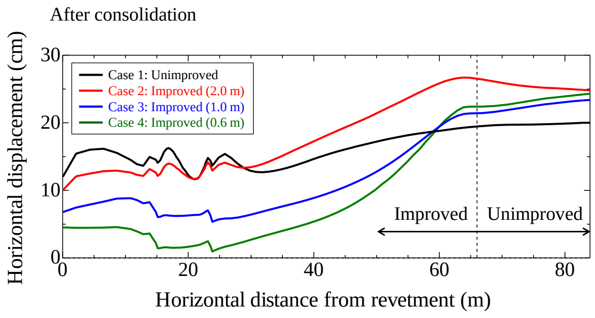

Figure 17 Horizontal displacement of ground surface (leftward displacement is positive)

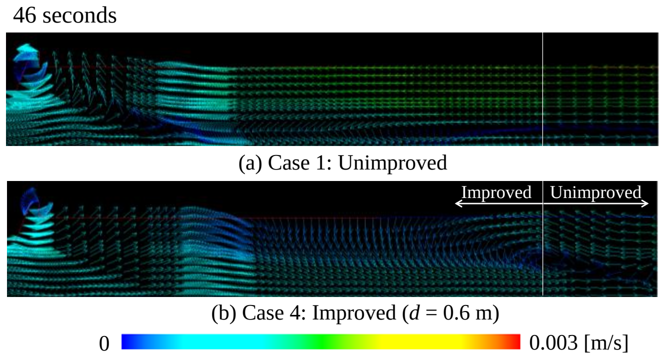

Figure 18 Distributions of velocity vector

The evaluation of ground deformation using a 1D mesh-based analysis is difficult in the vicinity of the revetment and the border between the improved and unimproved regions, as described earlier; therefore, a 2D mesh-based analysis is required. Evaluation using 2D mesh-based analysis is essential when considering ground deformations in the horizontal direction, such as lateral flows. Moreover, 3D mesh-based analysis is required when considering the ground deformation around building structures in more detail because these structures are represented as the status continuing in the depth direction when using the 2D plane-strain condition.

4. INFLUENCE OF THE PERMEABILITY COEFFICIENT OF THE DRAIN UPON THE IMPROVEMENT EFFECT

In the discussion up to this point, we have examined the influence of drain spacing on the improvement effect. However, the drain targeted in this study was assumed to be properly working because of its high permeability, and no cases have addressed how improperly working drains, i.e., the water pressure in the drain increases during the earthquake, would impact the improvement effect. The macro-element method expanded by the authors is capable of automatically reproducing the well resistance phenomenon based on the conditions of the drain. Utilizing this feature, the influence of well resistance upon the liquefaction-suppression effect on the reclaimed ground considered in this study was examined by conducting an analysis in which the permeability coefficient of drain was reduced. The permeability of the drain was assumed to have reduced because of drain clogging after construction. The effect of drain clogging is not considered in the current design. In this section, the usability of the macro-element method for maintenance is examined through numerical analysis.

4.1 Analytical examination using a 1D mesh

Figure 19 shows the relation between the permeability coefficient of the drain and maximum EPWP ratio. The drain-spacing cases considered were d = 1.0 m and 0.6 m. As explained in Section 3, these drain spacings were sufficient to obtain a liquefaction-suppressive effect. The maximum EPWP ratio was found at a depth of 6.5 m below the groundwater level.

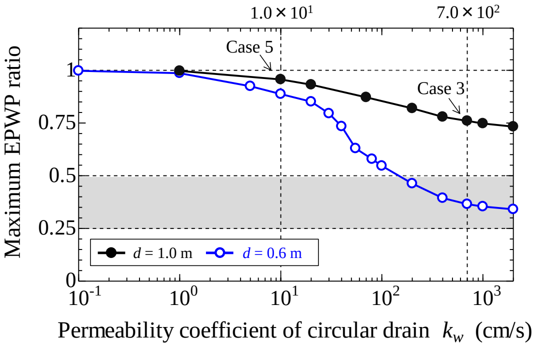

Figure 19 Relation between permeability coefficient of circular drain and maximum EPWP ratio

Lower the permeability coefficient of the drain, greater is the maximum EPWP ratio and less effective the suppression of liquefaction. Especially in the d = 0.6 m case, the improvement effect drastically dropped when the permeability coefficient of the drain decreased below 1.0×10^2 cm/s. Moreover, there was no suppression of liquefaction when the permeability coefficient of the drain reduced to 1.0×10^0 cm/s regardless of the drain spacing. The permeability coefficient of the drain generally used in PWPDM in Japan is in the range of 7.0×10^2–9.8×10^2 cm/s (Research Association for DEPP Method 2011). This is near the value where the maximum EPWP ratio converges; such values are ideal for obtaining the maximum benefit from these improvement effects.

Next, the water pressure in drain was validated. Case 5 (d = 1.0 m, $k_w = 1.0 \times 10^1$ cm/s), was targeted and its water pressure in the drain was compared with that of Case 3. Table 3 shows the analysis conditions.

Figure 20 presents the variation in the excess water pressure of the ground and drain in the depth direction. Since the permeability of the drain was low in Case 5, the water pressure of the drain was found to increase during an earthquake condition, resulting in the occurrence of well resistance. The suppression of the EPWP increase was not observed because of the well resistance. Thus, for the condition where the draining ability is insufficient, i.e., the drain has a low permeability coefficient or is narrow, the macro-element method proposed by the authors (Yamada et al. 2015; Noda et al. 2015), in which water pressure of drain is treated as unknown, is capable of automatically reproducing the phenomenon of well resistance in line with the mechanism of the occurrence of it. In the original formulation of the macro-element method (Sekiguchi et al. 1986), water pressure in the drain was specified by the analyst/investigator as an analytical condition, thus making it difficult to consider these effects of well resistance in the original method.

4.2 Analytical examination using a 2D mesh

The effect of the reduction of the drain's permeability coefficient on the suppression effect of ground deformation was examined in detail. Similar to that done for the results of 1D mesh-based analysis, the results of Case 5 were compared with those of Case 3.

Figure 21 shows the EPWP distributions for 150 s after an earthquake. Little suppression of the increase in EPWP was observed throughout the improved region in Case 5, in which the permeability coefficient of drain was reduced.

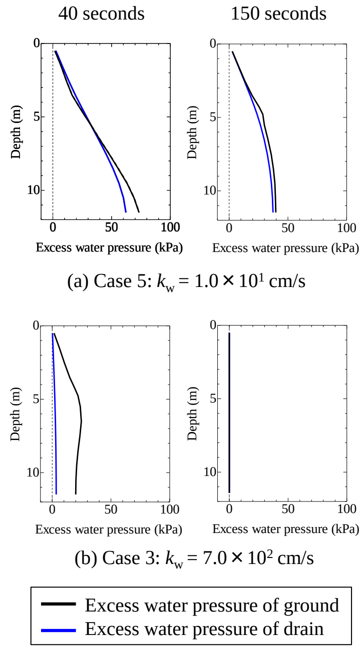

Figure 20 Excess water pressure in the depth direction

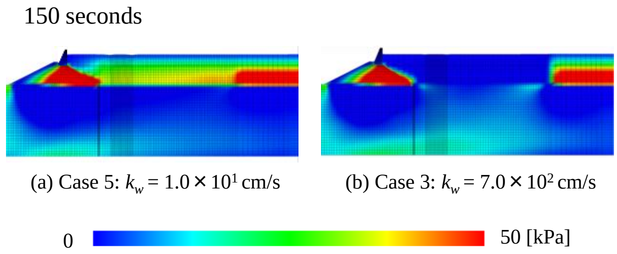

Figure 21 Distributions of EPWP

Figure 22 shows the settlements of the ground surface at the end of the earthquake and after consolidation. In Case 5, there was almost no suppression of the increase in EPWP during an earthquake and the stiffness of ground was reduced. Thus, there was no suppression of local settlement at places subjected to concentrated loads.

As shown by the above results, even for drain-spacing values sufficient for improving the reclaimed ground, if the permeability of the drain was significantly reduced because of drain clogging or other factors, much of the anticipated benefit from the drain system was observed to have been lost. Thus, well resistance occurring in drains had a great impact on the improvement effect of PWPDM. Therefore, it is essential to take measures to prevent the drain clogging after construction. The new macro-element method is capable of quantitatively evaluating the suppressive effect of liquefaction in the case where the permeability of the drain is reduced and is also useful for maintenance purposes.

5. PROPOSAL OF AN EFFICIENT DESIGN PROCEDURE FOR PWPDM

In this section, an efficient design procedure for PWPDM is proposed based on the findings in this study, utilizing the maximum advantage of the strengths of the new macro-element method.

[STEP 1: Narrow the range of the effective drain spacing (1D mesh-based analysis)]

The range of the effective drain spacing is narrowed in response to the needs of construction sites by not only suppressing the maximum EPWP ratio within the permissible range but also adequately evaluating the improvement effect in the horizontal bedding ground, such as the ground settlement without the influence of concentrated loads.

[STEP 2: Set the drain spacing (2D or 3D mesh-based analysis)]

The drain spacing can be adequately determined by evaluating the settlement and the horizontal deformation of ground around the locations that are under the concentrated loads of superstructure and in the vicinity of the border between improved and unimproved regions.

[STEP 3: Evaluation of maintenance of drain permeability performance (1D mesh-based analysis)]

To evaluate the maintenance of drain permeability by preventing drain clogging and other problems, the liquefaction-suppressive effect is examined quantitatively for the case where the permeability of the drain is reduced.

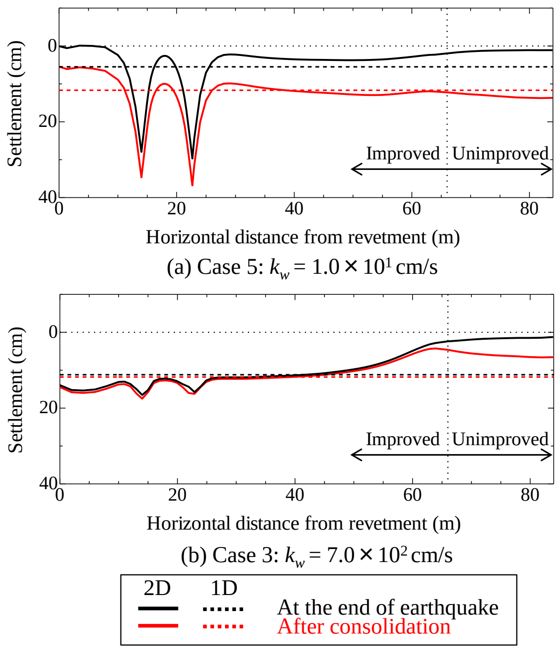

Figure 22 Settlement of ground surface

6. SUMMARY

The improvement effect of PWPDM was examined on reclaimed ground for a wide scale using ***GEOASIA*** with the new macro-element method. The authors attempted to quantitatively evaluate the suppressive effect of liquefaction in the case where the maximum EPWP ratio exceeded the permissible value specified in the current design code. Moreover, utilizing the feature of the new macro-element method, the influence of well resistance phenomenon on the suppression effect of liquefaction was examined. The main findings are as follows:

1) The analysis code ***GEOASIA*** employing the new macro-element method was validated by the analytical results for ground surface settlement and the results agreed well with the results obtained by an empirical formula.
2) ***GEOASIA*** with the new macro-element method made it possible to quantitatively and effectively evaluate the improvement effect of PWPDM in an actual reclaimed ground even for a wide-scale analysis. The liquefaction-countermeasure effect of PWPDM is thus expected to be effective in an actual reclaimed ground like the region examined in this study.
3) As explained earlier, liquefaction countermeasures with the drain-spacing range based on the current design code may be more stringent than required to guarantee safety. More advanced performance design of PWPDM is possible by not only suppressing the maximum EPWP ratio within the permissible range but also adequately evaluating the ground deformation.
4) The evaluation of ground deformation using 1D mesh-based analysis was difficult in the vicinity of the revetment and border between the improved and unimproved regions, indicating the need for a 2D mesh-based analysis. Furthermore, the evaluation using 2D mesh-based analysis was essential when considering ground deformation in the horizontal direction, such as lateral flows.
5) When the permeability of the drain was insufficient, the water pressure in the drain increased. As a result, EPWP of the ground also increased, thereby liquefying the soil. Therefore, it is essential to maintain the drains such that their permeability coefficients do not decline. The new macro-element method was capable of reproducing the well resistance effects. Therefore, this method is useful for maintenance purposes.

7. ACKNOWLEDGEMENT

The authors express their deep gratitude to the Japan Society for the Promotion of Science for their support to this study with Grant-in-Aid for Scientific Research (A) 25249064.

Appendix A. Application of the macro-element method to a soil-water finite deformation analysis code with inertial terms (Noda et al. 2015)

The soil-water finite-deformation analysis with inertial terms developed by the authors (Noda et al. 2008) employs a so-called $\boldsymbol{u}$-p formulation to obtain the nodal-displacement-velocity vector $\{\boldsymbol{v}^N\}$ and a representative pore water value u for each element by solving the space-discretized rate-type equation of motion and a soil-water coupled equation given by:

$$\mathrm{M}\{\dot{\boldsymbol{v}}^N\} + \mathrm{K}\{\boldsymbol{v}^N\} - \mathrm{L}^{\mathrm{T}}\dot{u} = \{\dot{\boldsymbol{f}}\} \tag{A1}$$

$$\frac{k}{g}\mathrm{L}\{\dot{\boldsymbol{v}}^N\} - \mathrm{L}\{\boldsymbol{v}^N\} = \sum_{i=1}^{m} \alpha_i (h - h_i)\,\rho_w g \tag{A2}$$

where M is the mass matrix, K is the tangent stiffness matrix, L is the matrix for converting $\{\boldsymbol{v}^N\}$ to the elemental volume-change rate, $\{\dot{\boldsymbol{f}}\}$ is the material time derivative of the equivalent nodal force vector, h and h_i represent the total heads corresponding to the representative values of water pressure for a given element and for adjacent elements, respectively, k is the permeability coefficient for the ground, g is the magnitude of gravitational acceleration, α_i is the coefficient of pore water flow to adjacent elements, ρ_w is the density of water, and m is the number of boundary surfaces for each element. The first term on the left-hand side of Eqs. (A1) and (A2) is the inertial term. The compressibility of water has been ignored for simplicity.

Next, the previously developed macro-element method with water absorption and discharge functions for vertical drains (Yamada et al. 2015) was applied to the analytical method above. First, we applied the following soil-to-drain pore water flow model to each element:

$$\dot{Q}_D = \kappa(u - u_D)\big(= \kappa(h - h_D)\rho_w g\big) \tag{A3}$$

$$\kappa = \frac{8kV}{F(n)d_e^2\rho_w g} \tag{A4}$$

$$F(n) = \frac{n^2}{n^2-1}\ln n,\ \ \frac{3n^2-1}{4n^2},\ \ n = \frac{d_e}{d_w} \tag{A5}$$

where $\dot{Q}_D$ is the soil-to-drain pore water flow rate, κ is the coefficient of pore water flow from the soil to the drain, u_D is the representative value for water pressure in the drain for each element, h and h_D are the total heads corresponding to u and u_D, respectively, and V is the current volume of each element. d_e and d_w represent the equivalent diameter and the diameter of the circular drain, respectively, and are treated as material constants.

To incorporate the water-absorption function of vertical drains into each element, Eq. (A3) is added to the right-hand side of Eq. (A2), yielding the following expression:

$$\frac{k}{g}\mathrm{L}\{\dot{\boldsymbol{v}}^N\} - \mathrm{L}\{\boldsymbol{v}^N\} = \sum_{i=1}^{m}\alpha_i(h-h_i)\,\rho_w g + \kappa(h-h_D)\rho_w g \tag{A6}$$

Eq. (A6) is called the soil-water continuity equation and replaces Eq. (A2) as the governing equation.

In the original formulation of the macro-element method (Sekiguchi et al. 1986), u_D or h_D was specified by the analyst/investigator as an analytical condition. However, the authors recently proposed treating this value as an unknown. The following continuity equation for the drain, which is virtually included in the macro element, is formulated to compensate as many equations as the increased unknowns under the assumption that the mesh division from the top to the bottom of the improved region is initially done approximately vertically:

$$\kappa(h-h_D)\rho_w g = \sum_{j=1}^{2}\beta_j(h-h_{Dj})\rho_w g \tag{A7}$$

where, β_j is the coefficient of water flow through the virtual drain contained in each element and h_{Dj} is the total head of the drain contained in the elements above and below the macro element. For the sake of simplicity, it is assumed that water flow through the drain obeys Darcy's law. Bearing in mind that the ratio of the cross-sectional area of the virtual drain to the area of the boundary surface between the elements connected above and below is $1/n^2$; β_j is given by the following equation:

$$\beta_j = \frac{k_w}{l^j}\frac{\boldsymbol{l}^j}{l^j}\cdot\boldsymbol{n}^j\frac{s^j}{n^2} \tag{A8}$$

where each symbol is defined as illustrated in Figure A1. k_w is the permeability coefficient for a circular drain and is treated as a material constant. The discharge function of the drains is incorporated into the macro-element method by treating the water pressure in the drain as an unknown while simultaneously adding Eq. (A7) as a governing equation. The boundary conditions for Eq. (A7) are handled in the same manner as the hydraulic boundary conditions for Eq. (A2). The initial value of the water pressure in the drain is to be matched with the pore water pressure at the point when the macro-element method is applied, unless there is a specific reason for not doing the same.

Ultimately, Eqs. (A1), (A6), and (A7) represent the governing equations when the macro-element method is applied. Solving these equations simultaneously yields $\{\boldsymbol{v}^N\}$, u, and u_D. As implied by the fact that Eq. (A1) is used as it is, we assume that the effect of the vertical drain's presence on the element's rigidity and mass is negligible. In addition, we assume that the change in drain volume in Eqs. (A6) and (A7) is sufficiently small relative to the change in ground volume.

One noteworthy feature of the macro-element method introduced above is that the mesh division can be specified independently of drain arrangement and drain pitch. As reported in Yamada et al. (2015), the supplementary conditions for the original macro-element method proposed by Sekiguchi et al. (1986, 1988) are not necessary. For a detailed explanation of how the material constants d_e, d_w, and k_w are determined, see Yamada et al. (2015).
In addition, for analyses based on ***u**-p* formulation, there is an upper limit on the permeability coefficient in terms of the time increment per step (Noda et al. 2008). Although this upper limit can hinder calculations when the drain is represented using a divided mesh, the drain permeability coefficient in the macro-element method is not subject to such constraints. For analyses based on the ***u**-p* formulation, this point along with the improved calculation efficiency can be emphasized as merits of the macro-element method.

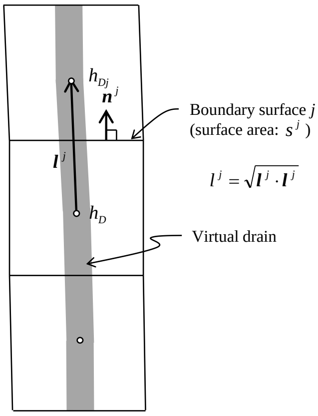

Figure A1 Virtual drain contained in mesh elements

Appendix B. The empirical formula for ground surface settlement with PWPDM

The empirical formula for settlement of the ground surface with PWPDM is illustrated, as proposed by Ono et al. (2009) and Unno et al. (2014), on the basis of the results of 1G shaking-table tests. At first, by applying Darcy's law within a confined aquifer, discharge per one drain q is shown as Eq. (B1) as follows, using the radius of the circular drain r_w and the permissible EPWP ratio $(u_{max}/\sigma'_v)_{ave}$:

$$q = \frac{2\pi k_s m(u_{max}/\sigma'_v)_{ave}\sigma'}{\gamma_w ln(r_0/r_w)} \tag{B1}$$

where k_s is the permeability coefficient of the ground, m is the layer thickness of the ground where the drain is installed, σ' is the average effective overburden pressure of the ground where the drain is installed (before the earthquake), γ_w is the unit weight of water, and r_0 is the distance from the center of the drain where the pore water pressure of ground is constant. This is calculated from Eq. (B2) as an empirical formula based on the result of shaking-table tests:

$$\frac{r_0}{r_w} = 1.56(u_{max}/\sigma'_v)_{ave}^{-0.10} \tag{B2}$$

The settlement of the ground surface caused by drainage during earthquake S is calculated as shown in Eq. (B3) using Eqs. (B1) and Eq. (B2):

$$S = \frac{qt}{\pi b^2} = \frac{2k_s m(u_{max}/\sigma'_v)_{ave}\sigma' t}{b^2\gamma_w ln[1.56\cdot(u_{max}/\sigma'_v)_{ave}^{-0.10}]} \tag{B3}$$

where b is the equivalent radius of the drain and t is the equivalent duration of earthquake.

Using the time factor T_l that represents the liquefaction resistance of the ground and the well resistance coefficient R (Yoshikuni et al. 1974) that represents the drainage resistance of the drain as a parameter, the permissible EPWP ratio $\left(u_{max}/\sigma'_v\right)_{ave}$ is decided using the design chart (Onoue 1988), which shows the relation between the permissible EPWP ratio $\left(u_{max}/\sigma'_v\right)_{ave}$ and the ratio of pile diameter, *a/b:*

$$T_l = \frac{k_s t_l}{m_v \gamma_w a^2} \tag{B4}$$

$$R = \frac{8}{\pi^2}\frac{k_s}{k_d}\left(\frac{h}{a}\right)^2 \tag{B5}$$

where m_v is the coefficient of volume compressibility, a is the radius of the circular drain, h is the installed depth of the drain, and k_d is the permeability coefficient of the drain. An example of the design chart is shown in Figure B1. For example, in Case 4 of Table 3, T_l, R, and a/b are calculated to be 517, 0.27, and 0.145, respectively; therefore, $\left(u_{max}/\sigma'_v\right)_{ave}$ is obtained as 0.09. By substituting this value into Eq. (B3), the settlement value S is calculated as 11.9 cm (the settlement S calculated using 1D mesh-based analysis with the macro-element method is 10.3 cm).

a/b	T_l=50	T_l=100	T_l=200	T_l=400	T_l=800	T_l=1200	T_l=1600	T_l=2000
0. 020	0. 9699	0. 9463	0. 9028	0. 8441	0. 7666	0. 7103	0. 6642	0. 6247
0. 025	0. 9537	0. 9154	0. 8614	0. 7889	0. 6936	0. 6244	0. 5686	0. 5220
0. 030	0. 9336	0. 8848	0. 8195	0. 7338	0. 6210	0. 5407	0. 4783	0. 4281
0. 035	0. 9096	0. 8532	0. 7776	0. 6787	0. 5500	0. 4621	0. 3971	0. 3474
0. 040	0. 8864	0. 8212	0. 7358	0. 6239	0. 4822	0. 3911	0. 3276	0. 2815
0. 045	0. 8623	0. 7892	0. 6939	0. 5698	0. 4195	0. 3294	0. 2706	0. 2299
0. 050	0. 8378	0. 7572	0. 6521	0. 5172	0. 3630	0. 2777	0. 2252	0. 1904
0. 055	0. 8132	0. 7252	0. 6105	0. 4670	0. 3135	0. 2352	0. 1895	0. 1600
0. 060	0. 7885	0. 6931	0. 5694	0. 4197	0. 2711	0. 2010	0. 1616	0. 1366
0. 065	0. 7638	0. 6610	0. 5291	0. 3760	0. 2353	0. 1734	0. 1395	0. 1180
0. 070	0. 7391	0. 6291	0. 4900	0. 3362	0. 2055	0. 1512	0. 1218	0. 1031
0. 075	0. 7144	0. 5973	0. 4524	0. 3004	0. 1808	0. 1331	0. 1073	0. 0909
0. 080	0. 6896	0. 5658	0. 4165	0. 2688	0. 1602	0. 1181	0. 0953	0. 0807
0. 085	0. 6648	0. 5347	0. 3828	0. 2410	0. 1429	0. 1055	0. 0852	0. 0722
0. 090	0. 6400	0. 5043	0. 3512	0. 2167	0. 1284	0. 0949	0. 0766	0. 0649
0. 095	0. 6153	0. 4747	0. 3220	0. 1957	0. 1160	0. 0858	0. 0693	0. 0587
0. 100	0. 5907	0. 4460	0. 2952	0. 1774	0. 1053	0. 0779	0. 0629	0. 0533
0. 110	0. 5422	0. 3918	0. 2486	0. 1476	0. 0879	0. 0651	0. 0525	0. 0444
0. 120	0. 4949	0. 3427	0. 2107	0. 1248	0. 0745	0. 0551	0. 0444	0. 0375
0. 130	0. 4495	0. 2991	0. 1801	0. 1069	0. 0638	0. 0472	0. 0380	0. 0320
0. 140	0. 4064	0. 2613	0. 1555	0. 0925	0. 0552	0. 0407	0. 0328	0. 0276
0. 150	0. 3662	0. 2288	0. 1356	0. 0808	0. 0482	0. 0355	0. 0285	0. 0240
0. 160	0. 3292	0. 2012	0. 1192	0. 0711	0. 0424	0. 0311	0. 0249	0. 0209
0. 170	0. 2956	0. 1779	0. 1055	0. 0630	0. 0375	0. 0275	0. 0220	0. 0184
0. 180	0. 2654	0. 1582	0. 0940	0. 0562	0. 0333	0. 0244	0. 0194	0. 0163
0. 190	0. 2386	0. 1415	0. 0843	0. 0503	0. 0297	0. 0217	0. 0173	0. 0145
0. 200	0. 2149	0. 1273	0. 0759	0. 0452	0. 0267	0. 0194	0. 0155	0. 0136
0. 220	0. 1760	0. 1044	0. 0623	0. 0370	0. 0217	0. 0157	0. 0133	0. 0121
0. 240	0. 1461	0. 0869	0. 0519	0. 0307	0. 0179	0. 0135	0. 0120	0. 0108
0. 260	0. 1229	0. 0733	0. 0437	0. 0257	0. 0149	0. 0123	0. 0107	0. 0095
0. 280	0. 1047	0. 0625	0. 0371	0. 0218	0. 0133	0. 0111	0. 0095	0. 0083

Figure B1 Design chart of PWPD (R = 0.30) (Research association for DEPP Method 2011)

8. REFERENCES

Adalier, K., Elgamal, A., Meneses, J. and Baez, I. J. (2003) “Stone columns as liquefaction countermeasure in non-plastic silty soils”, Journal of Soil Dynamics and Earthquake Engineering 23(7), pp 571-584.

Asaoka, A., Noda, T., Yamada, E., Kaneda, K. and Nakano, M. (2002) “An elasto-plastic description of two distinct volume change mechanisms of soils”, Soils and Foundations, 42(5), pp 47-57.

Cabinet Office. (2004) “Public data of Tonankai and Nankai earthquake”, (in Japanese).

Development group of liquefaction analysis code LIQCA. (2004) “Data of LIQCA2D04” (open to the public in 2004).

Howell, R., Rathje, E., Kamai, R. and Boulanger, R. (2012) “Centrifuge modeling of prefabricated vertical drains for liquefaction remediation”, Journal of Geotechnical and Geoenvironmental Engineering, 138(3), pp 262-271.

Kato, M., Oka, F., Yashima, A. and Tanaka, Y. (1994) “Dissipation of excess pore water pressure by gravel drain and its analysis”, Soils and Foundations, 42(4), pp 39-44 (in Japanese).

Lysmer, J. and Kuhleemeyer, R.L. (1969) “Finite dynamic model for infinite media”, American Society of Civil Engineers, Journal of the Engineering Mechanics Division, 95(4), pp 859-877.

Noda, T., Asaoka, A. and Yamada, S. (2005) “Elasto-plastic behavior of naturally deposited clay during/after sampling”, Soils and Foundations, 45(1), pp 51-64.

Noda, T., Asaoka, A. and Nakano, M. (2008) “Soil-water coupled finite deformation analysis based on a rate-type equation of motion incorporating the SYS Cam-clay model”, Soils and Foundations, 45(6), pp 771-790.

Noda, T., Asaoka, A. and Nakai, K. (2010) “Modeling and seismic response analysis of a reclaimed artificial ground”, Proceedings of Int. Conference on GeoShanghai 2010, Shanghai, pp 294-299.

Noda, T., Takeuchi, H., Nakai, K. and Asaoka, A. (2009) “Co-seismic and postseismic behavior of an alternately layered sand-clay ground and embankment system accompanied by soil disturbance”, Soils and Foundations, 49(5), pp 739-756.

Noda, T., Yamada, S., Nonaka, T. and Tashiro M. (2015) “Study on the pore water pressure dissipation method as a liquefaction countermeasure using soil-water coupled finite deformation analysis equipped with a macro element method”, Soils and Foundations 55(5), 1130-1139.

Ono, Y., Hayashi, K., Oota, M., Asada, H. and Yamazaki, H. (2009) “Effort to performance design of pore water pressure dissipation method”, Proceedings of symposium of the Construction Technology Research Committee in JSCE, Japan, pp 105-112 (in Japanese).

Onoue, A. (1988) “Diagrams considering well resistance for designing spacing ratio of gravel drains”, Soils and Foundations, 28(3), pp 160-168.

Oka, F., Yashima, A., Kato, M. and Sekiguchi, K. (1992) “A constitutive model for sand based on the non-linear kinematic hardening rule and its application”, Proceedings of 10th World Conference on Earthquake Engineering, Madrid, pp 2529-2534.

Papadimitriou, A., Moutsopoulou, M., Bouckovalas, G. and Brennan, A. (2007) “Numerical investigation of liquefaction mitigation using gravel drains”, Proceedings of 4th Int. Conference on Earthquake Geotechnical Engineering, Thessaloniki, paper No. 1548.

Research Association for DEPP Method. (2011) “Technical data on dissipation of excess pore water pressure method” (in Japanese).

Seed, H.B. and Booker, J.R. (1977) “Stabilization of potentially liquefiable sand deposits using gravel drains”, Journal of Geotechnical engineering division, American Society of Civil Engineers, 103(GT7), pp 568-757.

Sekiguchi, H., Shibata, T., Fujimoto, A. and Yamaguchi, H. (1986) “A macro-element approach to analyzing the plane strain behavior of soft foundation with vertical drains” Proceedings of the 31st symposium of the JGS, Japan, pp 111-116 (in Japanese).

Sekiguchi, H., Shibata, T., Mimura, M. and Sumikura, K. (1988) "Behaviour of the seawall and bridge abutment at the edge of an offshore airport fill", Annual report of Kyoto University, 32(B-2), pp 123-145.

Tanaka, Y. (1987) "A method to calculate excess pore pressures and surface settlements of the ground improved by gravel piles", Journal of Japan Society of Civil Engineers, 388(3-8), pp 23-32 (in Japanese).

Tanaka, Y., Kokusho, T., Esashi, Y. and Matsui, I. (1983) "Effects of gravel piles on stabilizing a sand deposit susceptible to liquefaction (2) -on the designing method of gravel piles with finite permeability-", Central Research Institute of Electric Power Industry Research Report No.382058, Central Research Institute of Electric Power Industry (in Japanese).

Tashiro, S., Asanuma, T., Oono, Y. and Hayashi, K. (2015) "Quantitative evaluation of drainage effect by the excess pore water pressure dissipation method in horizontal bedded ground during a large earthquake", Journal of Japan Society of Civil Engineers A1, 71(4), pp 145-158 (in Japanese).

Unno, T., Hayashi, K., Asada, H. and Iba, H. (2012) "Evaluation of the dissipation of excess pore water pressure method using centrifugal model test", Journal of Japan Society of Civil Engineers B3, 68(2), pp 480-485 (in Japanese).

Unno, T., Hayashi, K., Oono, Y., Asanuma, T., Sentoh, N. and Uzuoka, R. (2014) "Seismic deformation of improved ground with drainage during larger excess pore water pressure generation than the design value", Journal of Japan Society of Civil Engineers C, 70(1), pp 67-82 (in Japanese).

Yamada, S., Noda, T., Tashiro, M. and Nguyen, S. H. (2015) "Macro element method with water absorption and discharge functions for vertical drains", Soils and Foundations, 55(5), pp 1114-1129.

Yasui, M. and Yabunaka, K. (2002) "A transition of land reclamation policy in Japan", Journal of Japan Society of Civil Engineers B3, 18, pp 119-124 (in Japanese).

Yoshikuni, H. and Nakanodo, H. (1974) "Consolidation of soils by vertical drain wells with finite permeability", Soils and Foundations 14(2), pp 35-46.

Yoshimi, Y. and Fukutake, K. (2005) "Physics and evaluation, countermeasure technology of the ground liquefaction", Gihoudou Print Co. Ltd (in Japanese).